Bandwidth Extension of Acoustic Beamforming using Phase Unwrapping and Array Interpolation

Caleb B. Goates

A senior thesis submitted to the faculty of
Brigham Young University
in partial fulfillment of the requirements for the degree of

Bachelor of Science

Tracianne B. Neilsen and Kent L. Gee, Advisors

Department of Physics and Astronomy

Brigham Young University

April 2017

ABSTRACT

Bandwidth Extension of Acoustic Beamforming using
Phase Unwrapping and Array Interpolation

Caleb B. Goates
Department of Physics and Astronomy, BYU
Bachelor of Science

Acoustic beamforming uses recordings from a microphone array to find sound source locations. The response of a beamformer is limited by two requirements–the spatial Nyquist frequency on the high-frequency end and aperture requirements on the low-frequency end, which correspond respectively to the spacing of the microphones and the total length of the array. These limitations cause any array with a finite number of microphones to have a limited frequency bandwidth over which beamforming results are useful. This paper presents a method for overcoming the high-frequency limitation using phase unwrapping and array interpolation. This process can approximate the response of an array with many more microphones than are present by adding virtual microphone signals determined by interpolation. Experimental and numerical verifications of the method are presented. The method is found to octuple the bandwidth of the array when the source of interest is broadband.

Keywords: Beamforming, phase unwrapping, array interpolation, bandwidth extension

ACKNOWLEDGMENTS

I would like to start by thanking my advisor, Dr. Tracianne Neilsen, for her continual feedback on my research and thesis. She has been unwaveringly patient with me as I asked continual questions during the writing process. I would also like to thank Dr. Kent Gee for his encouragement and for introducing me to this project.

Most of all I would like to thank my wife for her support. She has learned enough about the topic of this thesis that she could follow along when I gave her updates on my progress, and she has expressed interest even when it must have been very uninteresting to her. I owe the success of this thesis to her.

Finally, I would like to thank the Office of Creative Research and Activities for supporting this project with an ORCA grant and the National Science Foundation and the Office of Naval Research for their support of the project as well.

Contents

List of Figures

Chapter 1

Introduction

In many noise control engineering, audio engineering, and sound propagation analysis situations it is important to be able to localize and characterize acoustic sources. A common way to do so is with acoustic beamforming. This thesis details the development of a method to overcome an inherent beamforming frequency bandwidth limitation using array interpolation and phase unwrapping. This chapter describes the current limitations on beamforming bandwidth and introduces the methods to be used.

1.1 Motivation

Beamforming is a method to localize sound sources [1] by phase shifting and averaging recorded signals from a microphone array. Standard delay-and-sum beamforming is illustrated in Fig. 1.1. In the example scenario shown in Fig. 1.1(a), there are two sound sources, indicated in blue and red, being recorded by five microphones, indicated by the gray circles. If the sources each emit a pulse, the signals received by the microphones are similar to Fig. 1.1(b), where each line represents a separate microphone signal. The signals are transformed into the frequency domain using a fast Fourier transform, and the phase shift $\varphi_i = \omega\tau_i$ is applied to each signal at each frequency, where

ω is the angular frequency, and τ_i is the time it takes the sound to travel from an assumed source location to the ith microphone. An assumed source position is chosen; we choose the location of the blue source and calculate each φ_i accordingly. If the signals are inverse Fourier transformed back into the time domain at this point, they will be aligned as shown in Fig. 1.1(c). Note that the blue signals are aligned, while the red signals are even less aligned than they were before due to the selected φ_i. The frequency-domain signals are then averaged. The time-domain representation of the averaged signals is shown in Fig. 1.1(d). The blue source signal averages to itself, while the red source signal averages out to have lower amplitude. In essence, beamforming is a spatial filter that can emphasize sound from an assumed source location while attenuating sound from all other locations [2]. If this process is repeated for several different scan locations (some of which may be locations of sound sources), the amplitude of the averaged signals can be plotted as a function of scan location to see where sources are located. These beamforming results are called source strength reconstructions, β.

Beamforming results depend upon the geometry of the array as well as the source locations. Beamforming is not a perfect process, showing large source amplitudes at scan locations where sources exist and zero amplitude everywhere else. An example of β for a single-source scenario is shown in Fig. 1.2(a). The source in this example is located at $X = 0$ m, and a scan was performed along a line that runs parallel to the array and includes the source. The lobe pattern that is shown, with a main lobe and several sidelobes, depends upon the spacing between array elements relative to a wavelength and the length of the array relative to a wavelength. If the array length is short relative to a wavelength, e.g., at a lower frequency, the main lobe becomes wider as shown in Fig. 1.2(b). The inverse is also true: As the array length becomes larger compared to a wavelength, the main lobe narrows. A narrow main lobe is desirable, as it increases the resolution of the beamforming results, allowing closely spaced sources to be resolved in β. Continuing to go higher in frequency does not give you an unlimited resolution with no strings attached, however. At

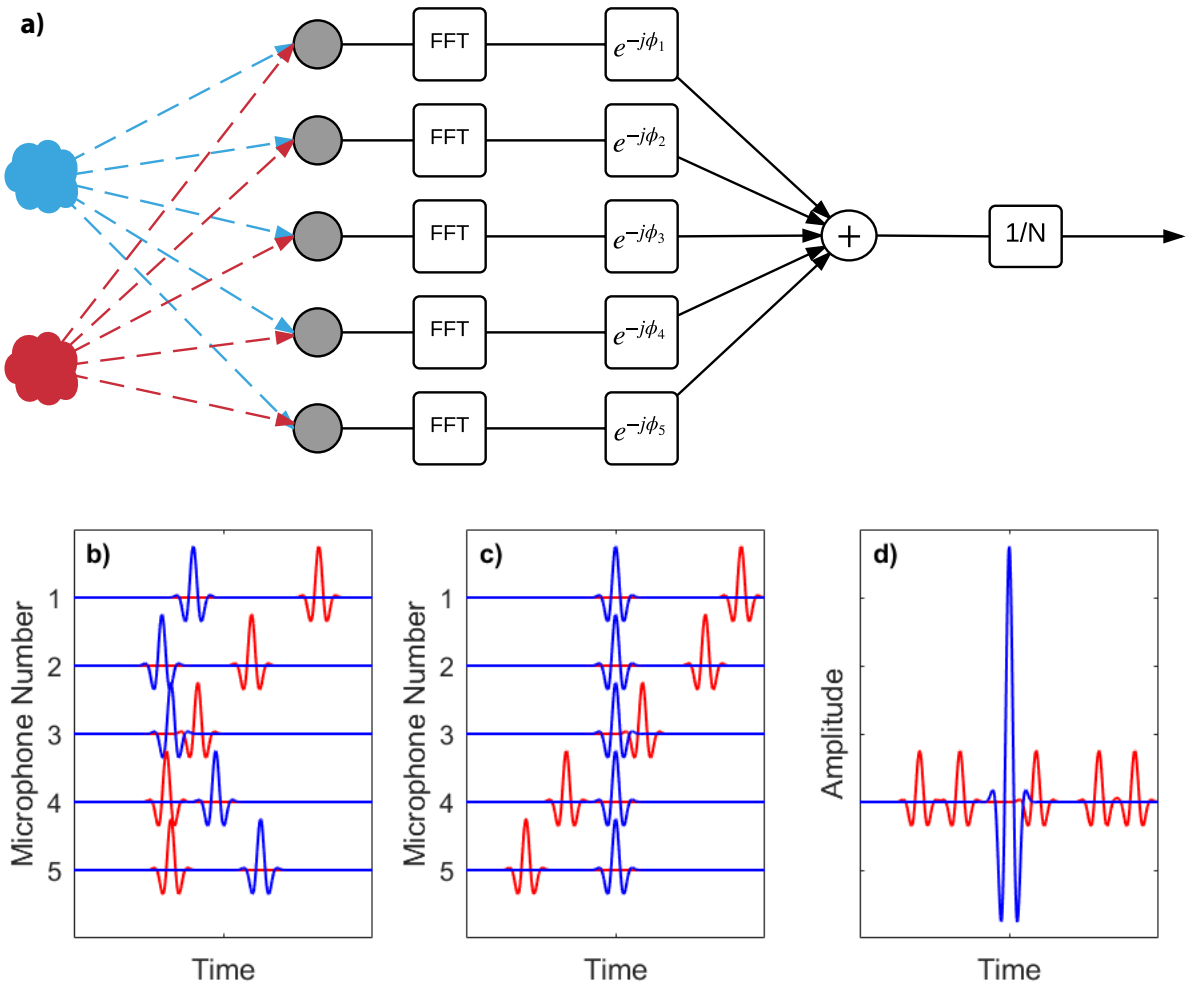

Figure 1.1 a) Pictoral representation of delay-and-sum beamforming in the frequency domain. Each signal is delayed by the amount of time it takes for sound to travel from the location of interest to the array, thus aligning the portion of each signal that came from that location. b) Signals received by each microphone from the red and blue sources depicted in part a), with each microphone on a separate line. c) Delayed signals to align the part of the signal coming from the blue source. d) The average of the delayed signals. The blue signal averages to itself, while the red signals average out to lower amplitude. Similar to figures in Ref. [3].

high frequencies the distance between the microphones comes into play. When the spacing of the microphones is greater than half a wavelength, false sources appear in β, as shown in Fig. 1.2(c). These false sources, called grating lobes, limit usable beamforming results to frequencies below that at which the microphone spacing is half a wavelength; this frequency is the spatial Nyquist frequency $f_N = c/2d$, where c is the speed of sound and d is the microphone separation.

Resolution requirements and grating lobes impose two opposite restrictions on a beamforming array that dictate the usable bandwidth. With a limited number of microphones, resolution at low frequencies calls for spreading them over a large aperture, while grating lobe avoidance at high frequencies calls for placing them close to each other. The result is that a single array configuration can only be used over a limited frequency bandwidth. This bandwidth limitation is the problem addressed in this thesis. Through phase unwrapping and array interpolation, we are able to overcome the grating lobe problem and increase the usable bandwidth of the array.

Several types of beamforming have been developed for various applications; our study focuses on conventional beamforming. Beamforming is used in underwater acoustics [4], audio acoustics [5], and aeroacousics [6], as well as outside of acoustics for applications such as radar [7], radio astronomy [8], and communications [9]. With such a variety of applications, beamforming has had many different variations developed. Conventional beamforming is a variation on the delay-and-sum beamforming described above. More detail on conventional beamforming is provided in Sec. 2.1.

Though this thesis focuses on conventional beamforming, there are other signal processing methods to which this work applies. These fall under the general name of phased-array techniques, and included in the list are several types of beamforming and acoustical holography, among others. Acoustical holography is not defined in this thesis; a good description may be found in Ref. [10]. The general idea is that there are limitations from having a finite number of microphones in each technique that can potentially be overcome using the methods presented in this thesis.

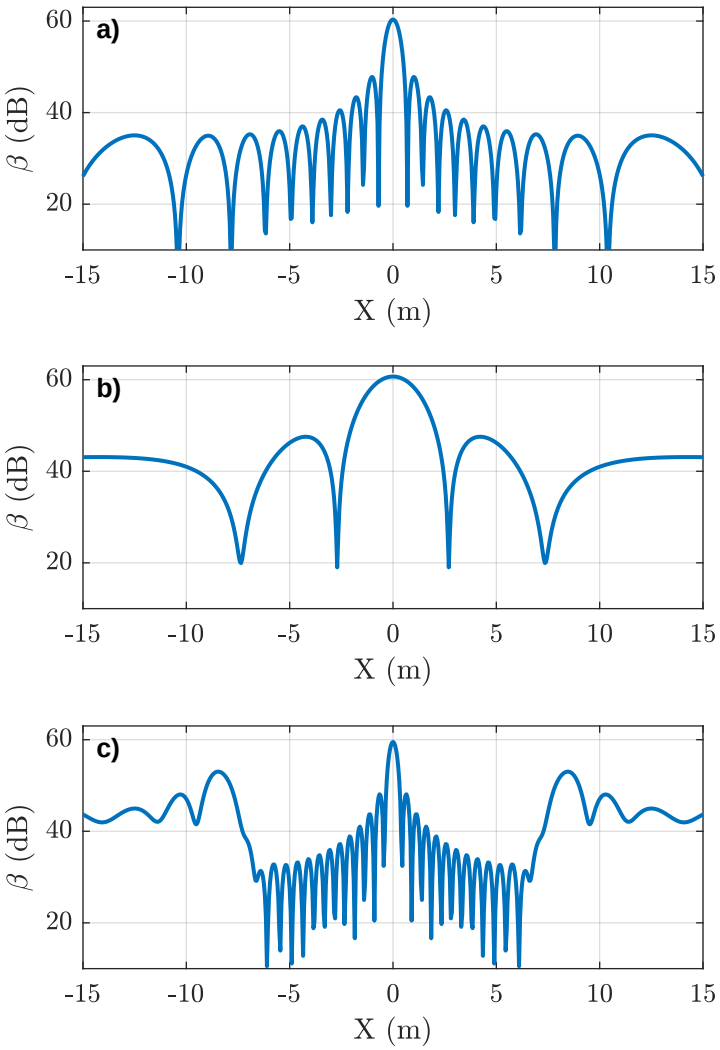

Figure 1.2 Examples of beamforming results for a single monopole at $X = 0$ m in three different frequency ranges. a) The beamforming pattern at a mid-range frequency. The main lobe is narrow and the side lobes are low. b) The beamforming pattern at a low frequency. The main lobe is wide, and the side lobes are low. This situation leads to poor spatial resolution in the beamforming results. c) The beamforming pattern at a high frequency, above the spatial Nyquist frequency. The main lobe is narrow, but false sources, called grating lobes, are present at $X = 8$ m and $X = -8$ m.

1.2 Array Interpolation

Array interpolation improves the results of beamforming through adding virtual microphones. Past work has used array interpolation to replace faulty microphones [11] [12], to lessen the effects of sensor noise [13], and to simulate an alternate array geometry [14]. Extrapolation has also been employed to increase the array aperture, thereby increasing the resolution of the results [11].

Common interpolation techniques are not able to operate above the spatial Nyquist frequency f_N, however. Interpolation is usually performed on real and imaginary parts of complex data, and can be done linearly, quadratically, or using linear prediction, but none of these techniques can give meaningful information above f_N. Traditionally, accurate interpolation requires the element spacing in the array to be less than half a wavelength [11].

The method presented in this thesis is able to perform array interpolation above f_N after implementing phase unwrapping. This is done by interpolating magnitude and unwrapped phase instead of complex pressures, as magnitude and unwrapped phase can often be assumed to vary smoothly.

1.3 Phase Unwrapping

Phase unwrapping is the process of computing the actual phase difference between two signals from the $[-\pi, \pi]$ constrained phase given by inverse trigonometric functions and phasor angles. An example of phase unwrapping where the phase varies linearly with frequency is shown in Fig. 1.3. In general, signals may have any phase difference between them, but as sinusoids have a 2π period, taking the argument of any complex number or the inverse of any trigonometric function gives a value between $-\pi$ and π. As a result, any time the phase goes outside of this range there is a 2π discontinuity, where the argument jumps from $-\pi$ to π, as illustrated by the black line in Fig. 1.3. One-dimensional phase unwrapping computes the actual, or unwrapped, phase $\tilde{\Phi}$ from

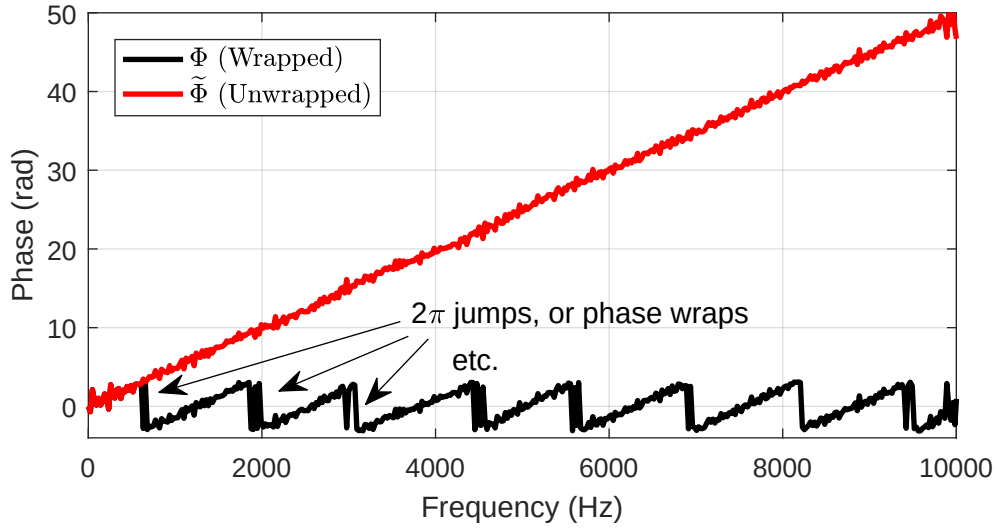

Figure 1.3 Wrapped and unwrapped phase difference between two microphones some distance apart in a propagating sound field. Initially, the phase is wrapped, with 2π jumps every time the phase goes outside the $[-\pi,\pi]$ range. At some frequencies, there are several 2π jumps next to each other caused by noise in the signal. Phase unwrapping removes all the discontinuities and recovers the linear absolute phase difference between the two microphones.

the wrapped phase Φ as

$$\tilde{\Phi}(f) = \Phi(f) + 2\pi\nu(f), \tag{1.1}$$

where $\nu(f)$ is an integer valued function, and f is frequency. This unwrapped phase is shown as the red line in Fig. 1.3.

Phase unwrapping is well researched and is used in several fields. Examples include radar [15], optics [16], robotics [17], speech processing [18], medical imaging [19], and communications [20]. Historically, the phase unwrapping problem has been an electrical engineering question, and often two-dimensional unwrapping is desirable because of the additional information afforded by the second dimension. A summary of common two-dimensional unwrapping techniques can be found in Ref. [21].

Previous work at BYU used phase unwrapping to overcome the spatial Nyquist frequency of acoustic intensity probes. Acoustic intensity is the flow of energy in sound, and traditional intensity

calculation is performed using a probe of two or more microphones. Accurate intensity estimation is limited by probe size to well below the spatial Nyquist frequency of the probe. A recently developed method [22] calculates intensity using the gradient of the phase and amplitude of the sound field; this method yields reliable intensity estimations up to the spatial Nyquist frequency, and beyond that if the phase difference between microphones is successfully unwrapped [23].

One-dimensional phase unwrapping techniques are being developed at BYU for intensity and beamforming applications specifically. While one-dimensional phase unwrapping lacks the additional information afforded by a second dimension, there are other ways to weigh the likelihood of correct unwrapping. Originally the current work and the intensity probe work used the MATLAB default phase unwrapping command, but it was insufficient for these applications, as false wraps were found and unwrapped in noisy signals. This work therefore switched to graduate student Mylan Cook's shooting method, which uses multiple points to determine when unwrapping has occurred [24]. Mylan Cook is also developing an unwrapping method that uses the coherence of the two signals to determine when wrapping is likely.

1.4 Overview

This paper presents the Unwrapped Phase Array INTerpolation (UPAINT) method to overcome a beamforming array's spatial Nyquist limitation. The beamforming algorithm is presented, along with a description of the problems encountered above f_N. When phase unwrapping is applied, array interpolation can add in the extra microphones needed to get meaningful results above f_N.

Two experimental verifications are presented: a single broadband source, and a source that changes position with frequency. Results show that in both cases the UPAINT method allows successful source localization at frequencies up to $8f_N$. A description of the UPAINT method and these experimental verifications has been published previously in Ref. [25].

Additional numerical studies are also presented to investigate application of UPAINT to extended sources and multiple point sources. UPAINT shows promise in extended source scenarios, such as jet noise. The simulations also suggest that the uncovering of a weak source hidden in a grating lobe may be possible.

Chapter 2

Methods

The Unwrapped Phase Array INTerpolation (UPAINT) method attempts to overcome the high-frequency limitation of a beamforming array, thereby increasing the usable bandwidth of the array. Here the math of the beamforming algorithm is presented, along with a more detailed description of the limitation UPAINT overcomes. The UPAINT method is then presented.

2.1 Conventional Beamforming

As mentioned previously, this paper focuses on the application of UPAINT to conventional beamforming. Conventional beamforming (CB) is an extension of the delay-and-sum algorithm described in Sec. 1.1. CB reconstructs source strength distributions using the cross spectral matrix $\boldsymbol{C}$ and steering vectors, which are defined in this section. This extension of delay-and-sum beamforming is useful because it incorporates time averaging.

The cross spectral matrix describes how several signals are related to each other at a specific frequency. For two time-dependent signals $x(t)$ and $y(t)$, where t is time, the cross spectrum, denoted as $G_{xy}(f)$, may be computed by taking the Fourier transform of each signal to obtain $X(f)$

and $Y(f)$, then multiplying one by the complex conjugate of the other:

$$G_{xy}(f) = X(f)Y(f)^*, \tag{2.1}$$

where * denotes complex conjugate. In practice, several $X(f)$ and $Y(f)$ pairs are calculated from smaller time segments of the signals, called blocks, and $G_{xy}(f)$ is calculated as an average over the blocks. The cross spectrum is a complex quantity; the magnitude, $|G_{xy}(f)|$, indicates how related the two signals are, and the phase, $\arg\{G_{xy}(f)\}$, is the phase difference between the two signals at frequency f. The cross spectrum between a signal and itself, i.e., $G_{xx}(f)$, is a real-valued mean-squared amplitude of the signal and is called the autospectrum. The cross spectral matrix at a specific frequency f_0 is the collection of all the cross spectra and autospectra for signals recorded by a microphone array and is defined as

$$\boldsymbol{C} = \begin{bmatrix} G_{11}(f_0) & G_{12}(f_0) & \dots & G_{1M}(f_0) \\ G_{21}(f_0) & G_{22}(f_0) & & \\ \vdots & & \ddots & \\ G_{M1}(f_0) & G_{M2}(f_0) & \dots & G_{MM}(f_0) \end{bmatrix}, \tag{2.2}$$

where $G_{ij}(f)$ is the cross spectrum between the ith and jth elements of the array, and M is the number of microphones. The information contained in the cross spectral matrix provides the source strength distribution β when the cross spectra are delayed and summed by multiplying the matrix by the steering vectors.

Steering vectors contain calculated phase shifts needed to propagate the signals from the microphones back to the scan location. A steering vector is defined as

$$e_n = \begin{bmatrix} e^{jkr_1} \\ e^{jkr_2} \\ \vdots \\ e^{jkr_M} \end{bmatrix}, \tag{2.3}$$

where r_i is the distance from the ith microphone to the nth scan point, and k is the acoustic wave number. The quantity kr_i represents the physical phase shift that the signal experiences as it propagates from the source to the ith microphone. The source strength β_n at the scan location represented by the steering vector is calculated as

$$\beta_n = e\boldsymbol{C}e^H, \tag{2.4}$$

where ^{H} is the conjugate transpose operator. The steering vectors propagate all of the cross spectra back to the scan locations. Any signal that originated from the scan location is added in phase and amplified. Signals that come from other locations are added as many randomly phase shifted copies, which in the limit as $M \to \infty$ averages to zero. The steering vectors are calculated and β_n is computed using Eq. 2.4 for each scan location. Ideally, the vector β of all β_n then contains a source strength distribution over the scan locations.

When $f_0 > f_N$, β may contain false sources, called grating lobes. This problem is caused by spatial aliasing and occurs when there are multiple locations that have the same or similar steering vectors, because the phase kr_i has wrapped. Figure 2.1 shows an example with two microphones in a plane wave situation. The black wavefronts in the left schematic reach the two microphones exactly in phase, so that it looks like there is no phase difference between the microphones. This is ambiguous, as it could just as well be the red wavefronts that cause the zero phase difference between the recorded signals. The ambiguity leads to the grating lobes in β, as shown in the right plot. The UPAINT technique interpolates $\boldsymbol{C}$ to supress these grating lobes.

2.2 The UPAINT Technique

The Unwrapped Phase Array INTerpolation (UPAINT) method interpolates the magnitude and phase of $\boldsymbol{C}$ separately. Because $\boldsymbol{C}$ is complex, two real-valued matrices may be obtained by separating the magnitude, $|\boldsymbol{C}|$, and phase, $\boldsymbol{\Phi} = \arg\{\boldsymbol{C}\}$, of $\boldsymbol{C}$. These $M \times M$ matrices can be interpolated

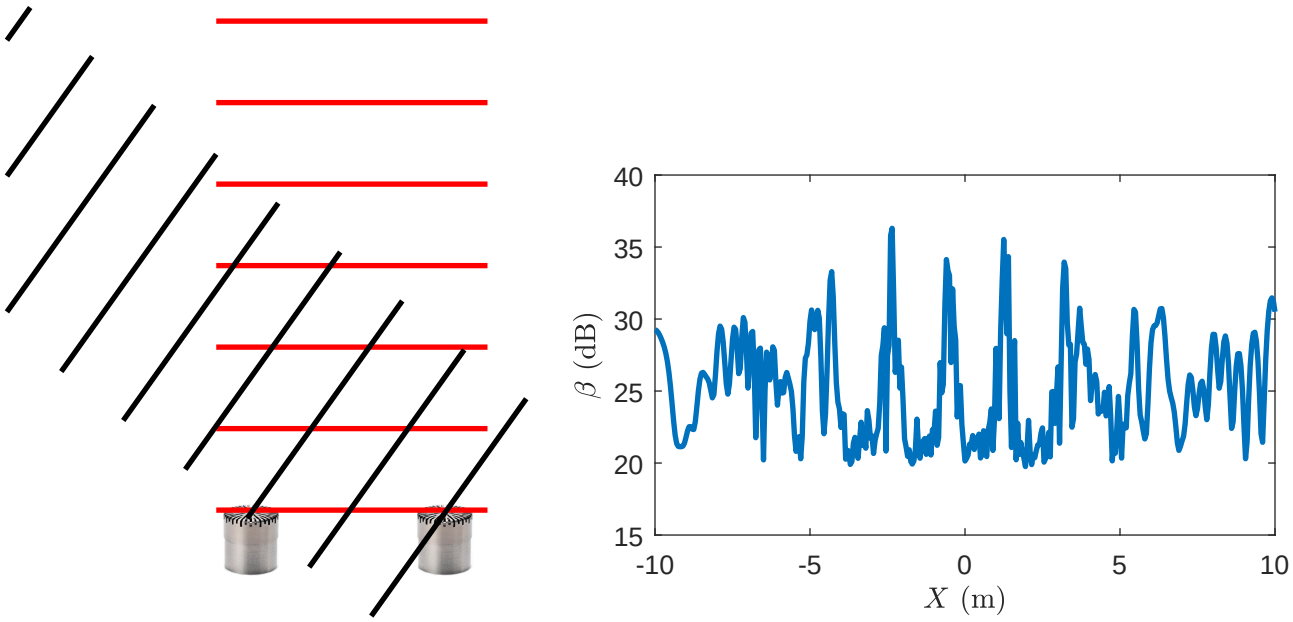

Figure 2.1 Grating lobes are false sources that appear when your microphone spacing is more than $\lambda/2$, or when $f_0 > f_N$. In the case shown in this figure, $f_0 \approx 5f_N$, and several grating lobes are present. These grating lobes occur when the phase difference between each of the microphones is the same, as shown in the left diagram. The left diagram shows wavefronts of the actual sound as black lines, and wavefronts of sound that has an equivalent steering vector as red lines, for a plane wave. An example of what this might look like in a source reconstruction is shown on the right. Though there is only one source present, multiple source-like peaks are present in β.

to $(M+N)\times(M+N)$ matrices representing an array containing N virtual microphones. By adding the virtual microphones between existing microphones, the effective spatial Nyquist frequency is increased.

Current interpolation methods act on the real and imaginary parts of $\boldsymbol{C}$, which do not vary smoothly. Examples of real and imaginary parts of $\boldsymbol{C}$ are shown in parts (a) and (b) of Fig. 2.2 at $f_0 = 2f_N$ for simulated measurements of a single point source on the line that perpendicularly bisects the array. This sinusoidal-like variation is typical of the real and imaginary parts. When $f_0 < f_N$, linear prediction is used to interpolate these quantities [11], modelling the spatial variation as a sum of sinusoids. For $f_0 > f_N$ these quantities may be aliased, producing incorrect interpolation. Standard data interpolation techniques other than linear prediction do not reproduce the sinusoid-like variations of the real and imaginary parts of $\boldsymbol{C}$ even for $f_0 < f_N$, except when the sound field is very well sampled, as most interpolation procedures are concerned only with creating a smooth transition between data points.

With phase unwrapping, the magnitude and phase vary smoothly and can easily be interpolated using any interpolation technique. The magnitude of the cross spectral matrix $|\boldsymbol{C}|$, an example of which is shown in Fig. 2.2(c), is more uniform than $\mathrm{Re}\{\boldsymbol{C}\}$ or $\mathrm{Im}\{\boldsymbol{C}\}$ in many cases. The phase of $\boldsymbol{C}$, or $\boldsymbol{\Phi}$, shown in Fig. 2.2(d), varies at least as much as $\mathrm{Re}\{\boldsymbol{C}\}$ and $\mathrm{Im}\{\boldsymbol{C}\}$ initially but with unwrapping also becomes smooth. Note that the only quantity that varies smoothly initially is the magnitude; the real and imaginary parts of $\boldsymbol{C}$ vary sinusoidally, and $\boldsymbol{\Phi}$ contains 2π discontinuities. An unwrapped phase $\widetilde{\boldsymbol{\Phi}}$ of $\boldsymbol{C}$ may be obtained as shown in Fig. 2.3: the phase of each $G_{ij}(f)$ is first unwrapped, as shown on the left, after which $\widetilde{\boldsymbol{\Phi}}$ is calculated from the values of the unwrapped phase at f_0, indicated by the oval and arrows. The calculated $\widetilde{\boldsymbol{\Phi}}$, shown on the bottom left, is smoothly varying; the smoothly varying $|\boldsymbol{C}|$ and $\widetilde{\boldsymbol{\Phi}}$ completely describe $\boldsymbol{C}$ and can be easily interpolated. Virtual microphones can thereby be added whether the frequency of interest is above or below f_N. A critical factor that determines the success of the method is whether each $\arg\{G_{ij}(f)\}$

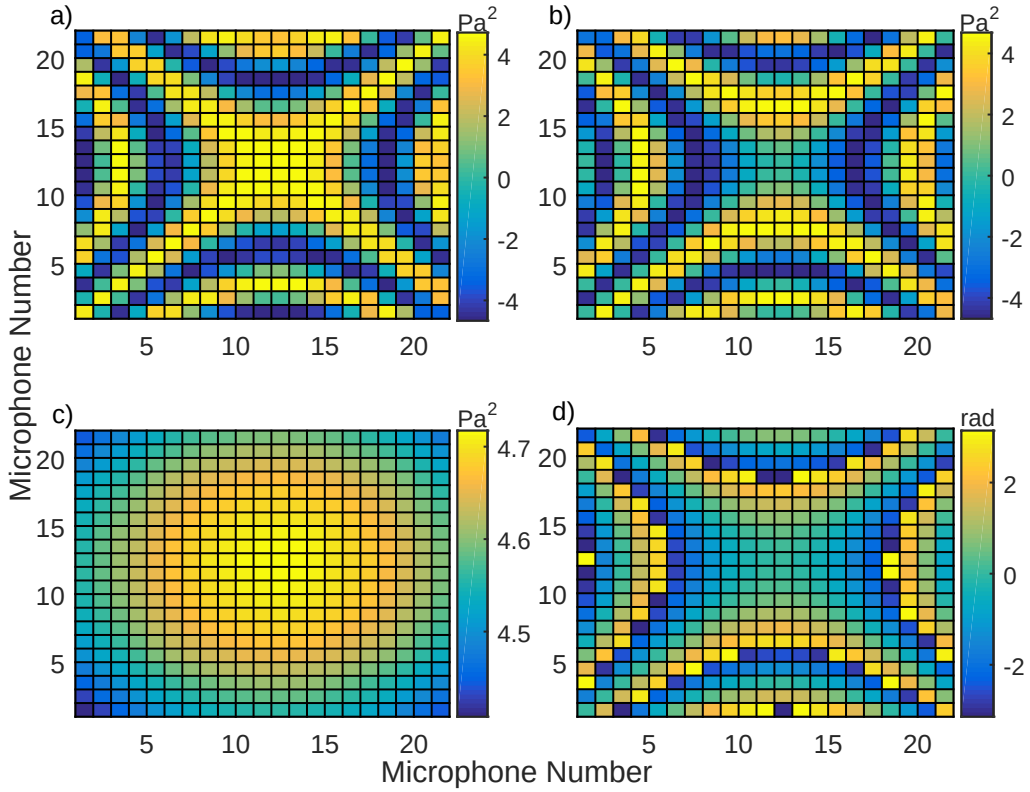

Figure 2.2 Examples of (a) the real part, (b) the imaginary part, (c) the magnitude, and (d) the phase of $\boldsymbol{C}$ for an array of 22 microphones recording the sound field from a single source on the line that perpendicularly bisects the array.

can be unwrapped.

At first, the MATLAB default unwrapping algorithm was used, but better results are obtained with other unwrapping algorithms. The MATLAB default algorithm simply defines the $\nu(f)$ function in Eq. 1.1 by adding or subtracting one from the value each time a jump of more than π is encountered in the phase. This can cause problems in a signal with an appreciable signal-to-noise ratio, however, as there may be spikes in the phase at certain frequencies, causing the $\nu(f)$ function, and consequently the unwrapped phase, to be incorrect for all frequencies above that at which the unwrapping error ocurred. Graduate student Mylan Cook has developed a shooting method algorithm that gives better immunity to these unwrapping errors by searching for a jump in the phase from an average of several previous points [24]. By implementing UPAINT with this algorithm, sucessful unwrapping and interpolation has been achieved for each $\arg\{G_{ij}(f)\}$ in the test cases presented in this thesis.

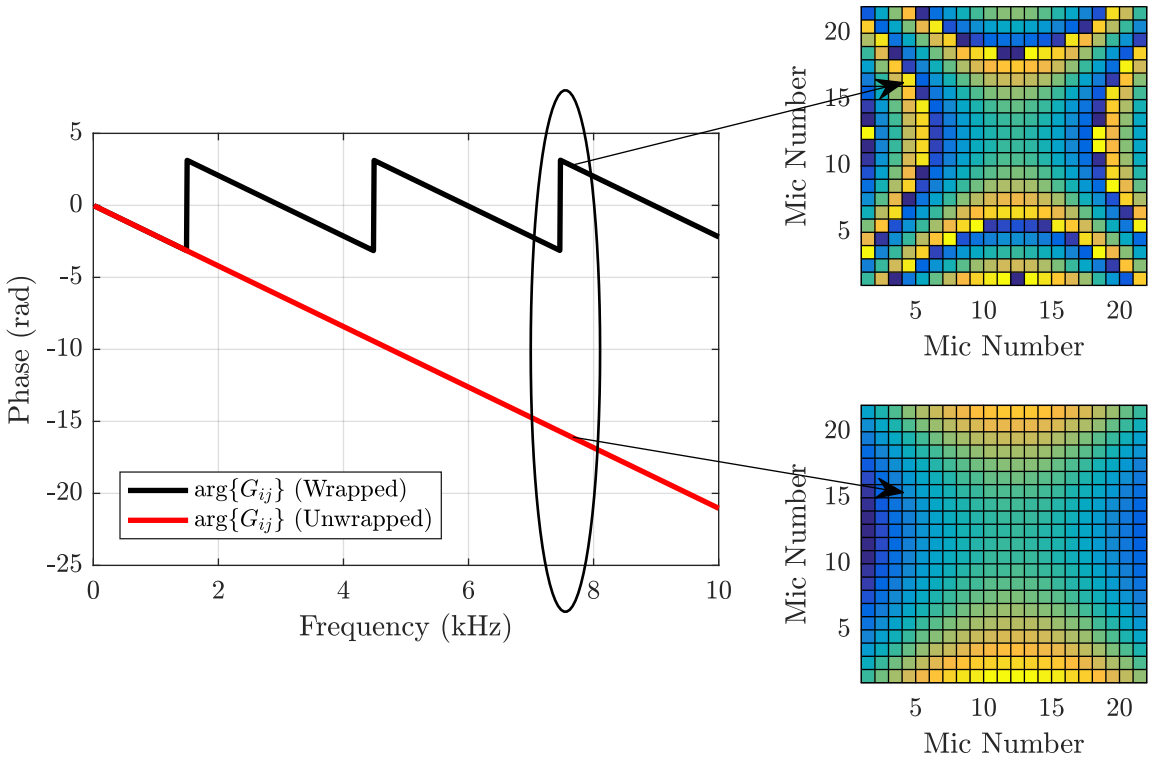

Figure 2.3 (Left) Example of wrapped and unwrapped phase for one pair of microphones. (Right) The phase of $\boldsymbol{C}$ at f_0, which is indicated by the oval in the left plot: $\boldsymbol{\Phi}$ (upper) and $\widetilde{\boldsymbol{\Phi}}$ (lower). Using the unwrapped phase of each cross spectrum at f_0, we can reconstruct the phase of $\boldsymbol{C}$ without the discontinuities.

Chapter 3

Results and Conclusions

Several studies are used to verify the viability of UPAINT; highlights are presented here. Two experimental cases are presented, followed by two numerical cases. In each case, conventional beamforming is performed with and without UPAINT applied as a preprocessing technique. Results are compared to see if grating lobes are suppressed by UPAINT.

3.1 Experimental Methods

Both of the experimental verifications shown here, denoted as experiments A and B, are performed in an anechoic chamber. A 22-element array is simulated using a stationary reference mic and a scanning mic. The scanning mic is moved to each location where an array microphone is desired, and the phase recorded by the mic is replaced by the phase difference between the stationary mic and the scanning mic. The effective array is designed with interelement spacing $d = 17$ cm, and $f_N = 1000$ Hz. The sources are placed along a line parallel to the array and 6.8 m away from it.

Two types of sources are used. Experiment A uses a single speaker playing broadband white noise located at the center of the scan line, which center we define as $X = 0$ m. Experiment B uses a more complex source, which, along with the setup of the array, is depicted in Fig. 3.1. This

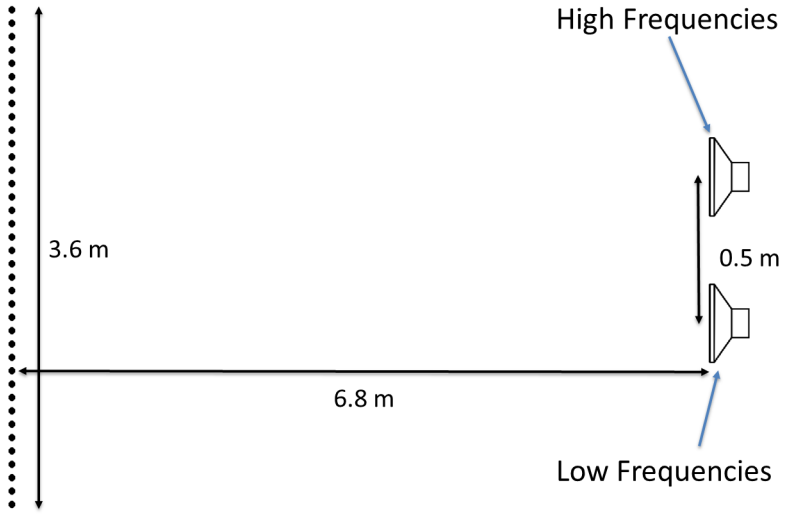

Figure 3.1 Setup and layout of experiment B. Two acoustic sources are separated by 0.5 m, and high frequencies are sent to one, while low frequencies are sent to the other. The setup is similar for experiment A, except that only one source is present.

source consists of broadband white noise sent through a crossover filter to two speakers separated by 50 cm, with the right speaker centered on $X = 0$ m. The crossover filter used is a digital implementation of a filter like that in a two-way loudspeaker that sends high frequencies to the tweeter and low frequencies to the woofer. The filter sends frequencies above the crossover frequency to the speaker on the left and frequencies lower than the crossover frequency to the speaker on the right. By filtering the signal in this way we simulate a source that radiates different frequencies from different locations, as many common sources do.

3.2 A single broadband source

Experiment A was an initial test of UPAINT with a single broadband source. This is the simplest scenario, and the one that should easily lend itself to successful phase unwrapping and interpolation, as the phase of each cross spectrum varies linearly with frequency. The beamforming results, β, are shown at two frequencies above f_N: Fig. 3.2(a) displays β at $2.5 f_N$, and Fig. 3.2(b) at

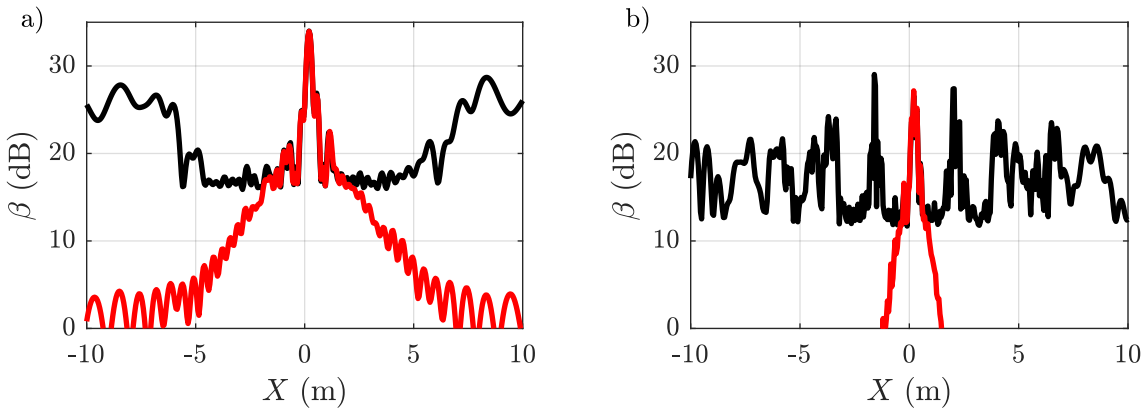

Figure 3.2 Beamforming results, β, for a single point source located at about $X = 0$ m, with and without UPAINT applied first for two frequencies: a) at $2.5f_N$; grating lobes are present at the edges of the scan area, but are stripped out after UPAINT is applied. b) at $8f_N$; grating lobes are abundant and look as reasonable as the actual source. UPAINT again strips out the grating lobes and locates the true source.

$8f_N$. Beamforming without UPAINT is shown in each case as a black line, and beamforming after UPAINT is applied is shown in red. In both cases there are grating lobes present initially. At $8f_N$, some of the grating lobes have higher amplitude than the actual source, making the possibility of guessing the correct source location with only that information impossible. The application of UPAINT before beamforming strips the grating lobes out and correctly identifies the true source location. In addition, the sidelobe levels are reduced significantly. This simple case is the first step in the verifications; UPAINT performs well here, leading us to investigate more complicated scenarios.

3.3 A source that changes location with frequency

Though a single speaker can be localized using only the frequencies below f_N (and thus not need UPAINT), many sources in practice do not have the same characteristics or location both above and below f_N. To simulate this situation in experiment B, the source that changes location with

frequency—described in Sec. 3.1—was used. This source was designed so that the crossover frequency, where the source changes location, would be above f_N of the array. Because of this, the second source location would be impossible to detect using only frequencies below f_N. Figure 3.3 shows the beamforming results at f_N as a gray dashed line, at $8f_N$ without UPAINT as the black line, and at $8f_N$ with UPAINT as the red line. Note that the horizontal axis in this figure is smaller than that in Fig. 3.2. If one had only the gray line and the black line, it would be impossible to tell which peak in the black line was the source location by comparing with the beamforming results at lower frequencies. There is no peak at the same location as there was at f_N, and the two closest peaks are equally viable options. When UPAINT is applied, however, the grating lobes are removed. The true source location at $8f_N$ is evident, and the characteristics of the source that are only described by the frequencies above f_N are recovered. Thus UPAINT processing can recover single sources from among grating lobes whether or not the sources change location with frequency.

3.4 Numerical simulations of multiple point sources

We performed numerical simulations to investigate the effectiveness of UPAINT in situations where multiple point sources are present. These simulations were designed to approximate the experimental setup described in Sec. 3.1: the array configuration is the same as previously described, and the simulation assumed an anechoic environment.

The results of these tests suggest a limitation in UPAINT. Multiple sources can cause the magnitude of the CSM to vary less smoothly, making it harder to interpolate. Figure 3.4 shows an example phase of a cross spectrum and an example $\mathbf{\Phi}$ matrix in an extreme case. This case, with widely spaced point sources in the far field, causes nulls in the magnitude and π jumps in the phase, making unwrapping impossible. The unwrapped phase shown on top has any number of equally

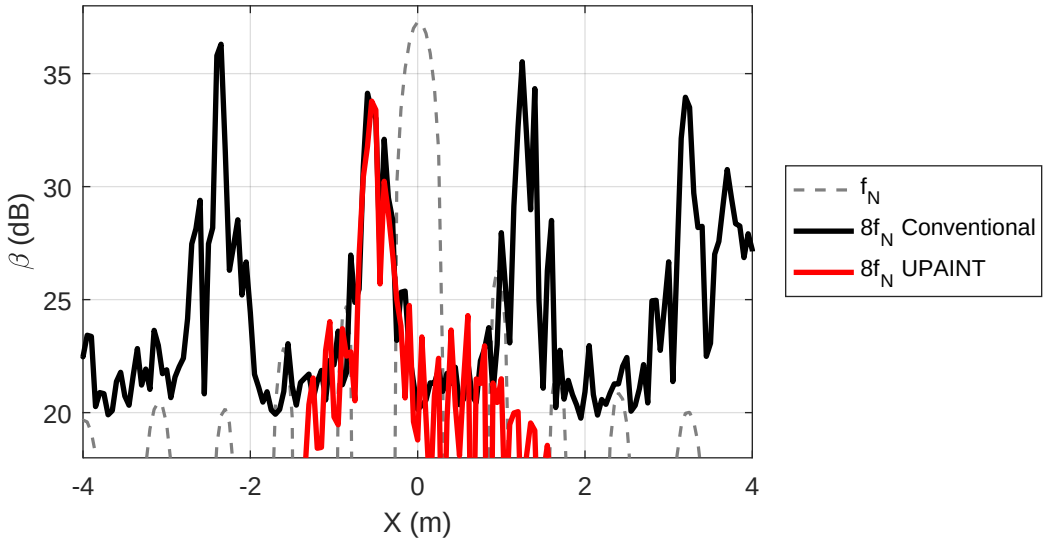

Figure 3.3 Beamforming results for a source that changes location with frequency. Results are shown at multiple frequencies on the same plot: the gray dashed line is the beamforming result at f_N, the black line is the result at $8f_N$ without UPAINT, and the red line is the result at $8f_N$ with UPAINT applied. Preprocessing with UPAINT strips out the grating lobes and allows the true source location at $8f_N$ to be recovered.

viable unwrapping options, and the unwrapping option that the algorithm chose is not correct. Below, Φ is shown before unwrapping. Though the phase varies smoothly in some sections of the matrix, the π discontinuities make interpolation impossible.

Though these results suggest poor prospects when multiple sources are present, more investigation is needed in this area. It could be that if the sources are within a small angular aperture they will not cause problems. Additional work also would need to adress near-field vs. far-field effects. In addition, better results seem to occur when one of the sources is an extended source.

3.5 Numerical simulation of an extended source

Two additional numerical simulations test the utility of UPAINT in situations involving a single extended source. These simulations were set up with 237 microphones evenly spaced over a 3.6 m array length. The source plane was 5 m away, and the tests were performed at $f_0 = 4.4 f_N$. Simulation A applies UPAINT to beamforming of a single extended source, and simulation B applies UPAINT to an extended source and a point source hidden in the grating lobe of the extended source.

In simulation A, UPAINT removes grating lobes and allows a single extended source to be localized. For this scenario, the extended self-coherent source spans a 2 m length from $X = -1$ m to $X = 1$ m, and has a Gaussian source strength distribution. Beamforming results β are shown in Fig. 3.5. In the beamforming without UPAINT, shown in black, there are two grating lobes present. When UPAINT is applied, the beamforming results, shown in red, mostly strip out the grating lobes. There are two peaks on the sides of the actual source that are artifacts of the UPAINT processing and not actual sources, but they are about 25 dB lower than the main source, and so are reasonably ignored.

Simulation B shows that it is possible to recover point sources hidden in grating lobes of ex-

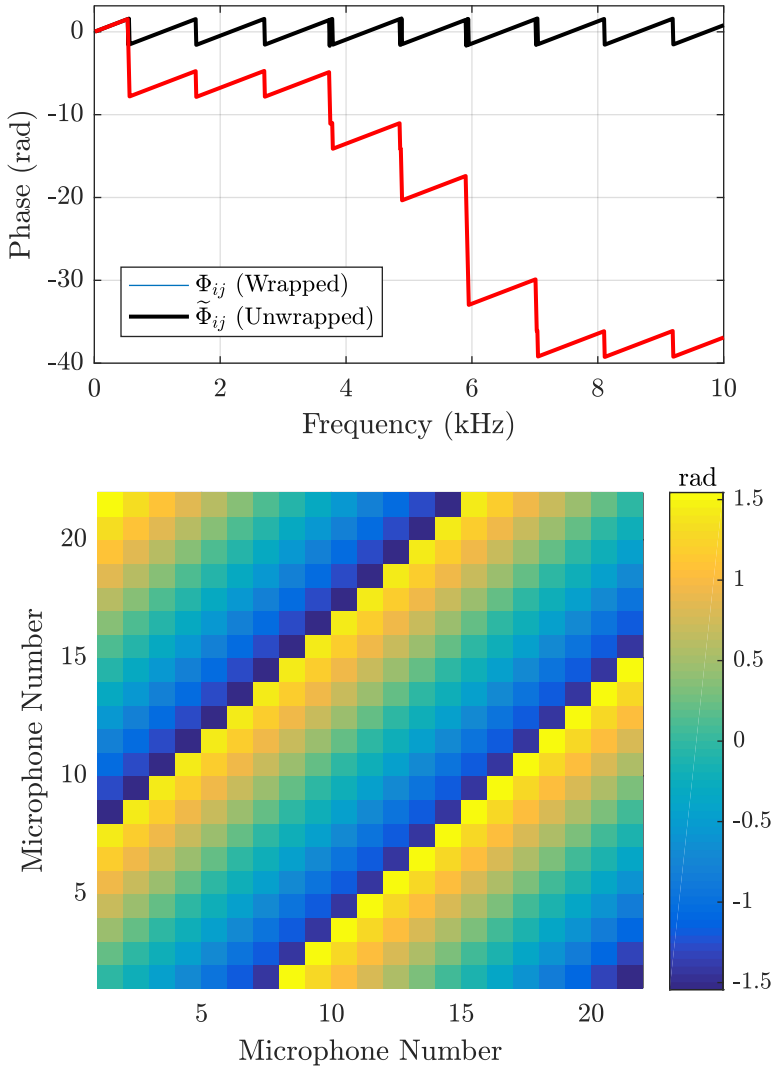

Figure 3.4 (Top) The phase of a cross spectrum that includes π jumps. Unwrapping in this case is impossible, as the unwrapping algorithm has no method to choose between keeping the π jump the way it is or unwrapping so that is is a π jump in the opposite direction. (Bottom) The wrapped phase $\mathbf{\Phi}$ corresponding to the cross spectrum above. The π discontinuities in $\mathbf{\Phi}$ make interpolation impossible, as the $\Phi_{ij}(f)$ cannot be unwrapped.

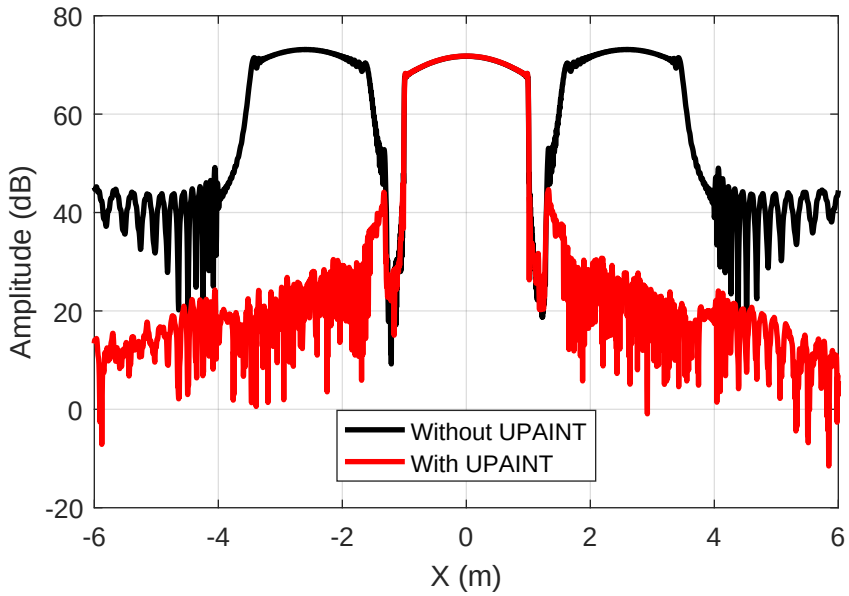

Figure 3.5 Beamforming results, β, for a numerical simulation of an extended source, with and without UPAINT applied. The extended source spans a 2 m length centered on the origin, with Gaussian source strength along that span. With UPAINT applied, grating lobes are removed and only the correct source remains.

tended sources. This simulation included a point source at $X = -1$ m and an extended source with Gaussian amplitude spanning from $X = 0$ m to $X = 1.5$ m. These positions were chosen so that the point source is within a grating lobe of the extended source at $f_0 = 4.4 f_N$. The beamforming results β are shown in Fig. 3.6. As in the last example, in the initial beamforming without UPAINT, shown in black, we see two grating lobes of the extended source, and these dominate β. With just this line, detection of the point source is impossible. UPAINT again strips out the grating lobes, however, leaving a peak in β (shown in red) at $X = -1$ m, the location of our hidden point source. The reconstruction gives a much lower source strength for the hidden source than was actually input to the simulation, but the location is correct, and the presence of the hidden source is detected.

The numerical simulations show that UPAINT is applicable to extended sources as well as point sources. This finding is useful for practical sources such as jet plumes and vibrating car doors. There are many situations in which practical sources are not reasonably approximated by point sources, and the utility of UPAINT in these scenarios is promising.

3.6 Concluding discussion

3.6.1 Conclusions

The UPAINT method is a preprocessing technique that allows removal of grating lobes above the spatial Nyquist frequency. Both experimental and numerical data show that using UPAINT extends the reliable bandwidth of beamforming source reconstruction for a single broadband source. In experimental verifications it was found that UPAINT can allow meaningful beamforming results up to $8 f_N$, increasing the bandwidth of a beamforming array by at least 7 times. Grating lobes were removed, and the correct source location was identified, whether the source radiated from the same location at all frequencies or changed location with frequency. Numerical studies show that

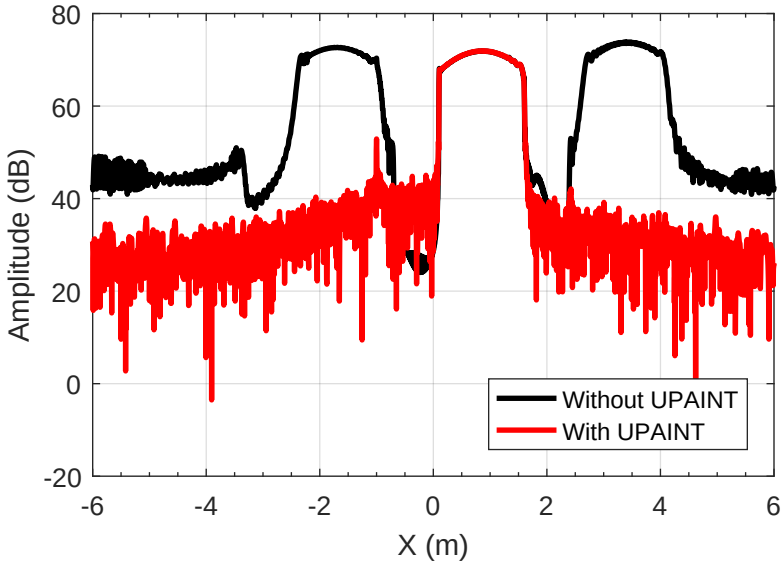

Figure 3.6 Beamforming results for numerical simulation of an extended source with a point source hidden in a grating lobe. The extended source spans a 1.5 m length, with gaussian source strength along that span. The point source is located at $X = -1$ m, inside a grating lobe of the extended source. Results are shown with and without UPAINT applied prior to beamforming. With UPAINT applied, the grating lobes are removed and the hidden source is located

UPAINT can also remove grating lobes for extended sources and suggest that sources hidden in grating lobes may be recovered.

3.6.2 Directions for further work

To assess the usefulness of UPAINT for multiple sources, more verifications are needed. It may be that if the sources are all within a small angular aperture the method will work well. Experimental verification of a practical source that includes multiple radiation locations, such as a blender or a leafblower, would be beneficial to the investigation of this question.

Application of UPAINT to jet noise, an extended source, is in process. This will continue previous work on jet noise characterization [26]. UPAINT will allow harvesting of much more information from previously acquired data using beamforming. Work on jet noise has included holography as well [27], and extension of UPAINT to acoustical holography should be investigated for these purposes.

Bibliography

[1] J. C. Chen, K. Yao, and R. E. Hudson, "Source localization and beamforming," IEEE Signal Processing Magazine **19,** 30–39 (2002).

[2] B. D. Van Veen and K. M. Buckley, "Beamforming: A versatile approach to spatial filtering," IEEE ASSP Magazine **5,** 4–24 (1988).

[3] S. P. Nasholm, "Conventional Beamforming,", Available at http://www.uio.no/studier/emner/matnat/ifi/INF5410/v12/undervisningsmateriale/foils/conventional_beamforming_part_1_plus_2.pdf (2017/04/11).

[4] R. J. Vaccaro, "The past, present, and the future of underwater acoustic signal processing," IEEE Signal Processing Magazine **15,** 21–51 (1998).

[5] F. Khalil, J. P. Jullien, and A. Gilloire, "Microphone array for sound pickup in teleconference systems," Journal of the Audio Engineering Society **42,** 691–700 (1994).

[6] X. Huang, L. Bai, I. Vinogradov, and E. Peers, "Adaptive beamforming for array signal processing in aeroacoustic measurements," The Journal of the Acoustical Society of America **131,** 2152–2161 (2012).

[7] P. Barton, "Digital beam forming for radar," IEE Proceedings F **127,** 266–277 (1980).

[8] K. F. Warnick, B. D. Jeffs, J. Landon, J. Waldron, D. Jones, J. R. Fisher, and R. Norrod, "Beamforming and imaging with the BYU/NRAO L-band 19-element phased array feed," 13th International Symposium on Antenna Technology and Applied Electromagnetics and the Canadian Radio Science Meeting **2009,** 1–4 (2009).

[9] L. C. Godara, "Application of antenna arrays to mobile communications. II. Beam-forming and direction-of-arrival considerations," Proceedings of the IEEE **85,** 1195–1245 (1997).

[10] E. G. Williams, *Fourier Acoustics : Sound Radiation and Nearfield Acoustical Holography* (Academic Press, San Diego, Calif, 1999).

[11] D. N. Swingler and R. S. Walker, "Line-array beamforming using linear prediction for aperture interpolation and extrapolation," IEEE Transactions on Acoustics, Speech, and Signal Processing **37,** 16–30 (1989).

[12] J. Hald, "Optimal interpolation of bad or non-existing measurement points in planar acoustical holography," Proceedings of InterNoise **2000,** 1–6 (2000).

[13] G. Doblinger, "Beamforming with optimized interpolated microphone arrays," Hands-Free Speech Communication and Microphone Arrays **2008,** 33–36 (2008).

[14] B. Friedlander, "The root-MUSIC algorithm for direction finding with interpolated arrays," Signal Processing **30,** 15–29 (1993).

[15] R. Gens, "Two-dimensional phase unwrapping for radar interferometry: developments and new challenges," International Journal of Remote Sensing **24,** 703–710 (2003).

[16] T. R. Judge and P. J. Bryanston-Cross, "A review of phase unwrapping techniques in fringe analysis," Optics and Lasers in Engineering **21,** 199–239 (1994).

[17] D. Li and S. E. Levinson, "A linear phase unwrapping method for binaural sound source localization on a robot," Proceedings of the IEEE International Conference on Robotics and Automation **2002,** 19–23 (2002).

[18] J. Kulmer, J. Stahl, and F. Mayer, *Single Channel Phase-Aware Signal Processing in Speech Communication: Theory and Practice* (John Wiley & Sons, 2016).

[19] S. Chavez, Q.-S. Xiang, and L. An, "Understanding phase maps in MRI: a new cutline phase unwrapping method," IEEE Transactions on Medical Imaging **21,** 966–977 (2002).

[20] H. F. Silverman, W. R. Patterson, and J. L. Flanagan, "The huge microphone array," IEEE Concurrency **6,** 36–46 (1998).

[21] D. C. Ghiglia and M. D. Pritt, *Two-dimensional phase unwrapping: theory, algorithms, and software* (Wiley New York, 1998), Vol. 4.

[22] D. C. Thomas, B. Y. Christensen, and K. L. Gee, "Phase and amplitude gradient method for the estimation of acoustic vector quantities," The Journal of the Acoustical Society of America **137,** 3366–3376 (2015).

[23] T. A. Stout, K. L. Gee, T. B. Neilsen, A. T. Wall, and M. M. James, "Source characterization of full-scale jet noise using acoustic intensity," Noise Control Engineering Journal **63,** 522–536 (2015).

[24] M. Cook, Master's thesis, Brigham Young University, Provo, Utah, United States, to be completed August 2018.

[25] C. B. Goates, B. M. Harker, T. B. Neilsen, and K. L. Gee, "Extending the bandwidth of an acoustic beamforming array using phase unwrapping and array interpolation," The Journal of the Acoustical Society of America **141,** EL407–EL412 (2017).

[26] B. M. Harker, T. B. Neilsen, K. L. Gee, A. T. Wall, and M. M. James, "Spatiotemporal-Correlation Analysis of Jet Noise from a High-Performance Military Aircraft," AIAA Journal **54,** 1554–1566 (2016).

[27] A. T. Wall, K. L. Gee, T. B. Neilsen, R. L. McKinley, and M. M. James, "Military jet noise source imaging using multisource statistically optimized near-field acoustical holography," The Journal of the Acoustical Society of America **139,** 1938–1950 (2016).

Index